THE TECHNOLOGICAL SIGNIFICANCE OF INTERACTIONS BETWEEN GASES AND GLASSES

LUBOMÍR NĚMEC, JAROSLAV KLOUŽEK, JIŘÍ ULLRICH*

Laboratory of Inorganic Materials,
Academy of Sciences of the Czech Republic and Institute of Chemical Technology,
Technická 5, 166 28 Prague
E-mail: nemec@iic.cas.cz

**Glass Service, Ltd., Vsetín*

Submitted April 9, 1998, accepted August 26, 1998.

INTRODUCTION

The technologically significant phenomena involving reactions of gases with glass occur in a broad temperature interval, starting from transformation interval up to refining temperatures. They engage at least six gases, namely CO_2, H_2O, O_2, SO_2, Ar, and N_2, and can be controlled by the mass or heat transfer, chemical reaction or nucleation. They deeply influence the rate of batch decomposition reactions, the properties of glass level by evaporation and foaming, the effectiveness of the refining process and consequently, the quality of resulting glass. The significant gas - glass phenomena are schematically shown in figure 1.

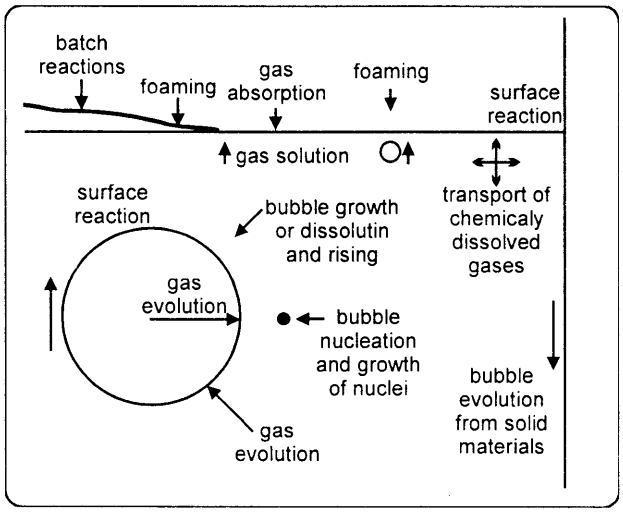

Figure 1. The schematic representation of gas-glass phenomena.

In order to optimize the process and to avoid bubble defects in glass, the appropriate theoretical models should be available and they have to be verified mostly by laboratory experiments and subsequently applied under technological conditions:

- reactions in the glass batch and foaming
- interaction of gases on the glass level
- interaction of bubbles with glass
- bubble nucleation in glass
- bubble evolution from solid materials
- interaction of bubbles with highly viscous and solid glass.

THE THEORETICAL MODELS OF GAS - GLASS INTERACTIONS

Reactions in the glass batch and foaming

Gas nucleation and gas evolution may be the rate controlling mechanisms of batch reactions already in the stage of solid state reactions in the glass batch. Consequently, the rate of batch conversion decreases when there is an increasing amount of batch [1]. During the stage of melt arising, the gases are stirring the melts but separate the dissolving particles. The size distribution of dissolving particles and the rate of heating influence mainly the saturation of the melt by gases and the initial composition and structure of bubbles and foam. The presence of refining agents intensifies this behaviour. Foaming in this stage can be reduced by driving off the batch gases before formation of viscous melt, by accelerating the gas release to the environment using fine silica, and by slow heating of coarse silica, by rapid heating, by additions of Na_2SO_4 or melting agents ($NaNO_3$) and by adjusting temperature gradients [2]. The role of sulphates consists in sulphate phase formation around sand particles under rapid heating, and, in every case, in bubble nucleation on the sand particles, which accelerates the sand dissolution by convection, adjusts foam formation in later stages, and controls the glass saturation by sulphates for the refining process [3]. No general theoretical model of gas release and functioning exists up to now.

Foam coming from the primary stage blocks the heat radiation. The foam is overheated as a consequence of

the low heat transfer from the combustion space. The viscosity of the foam increases due to evaporation and the foam is stabilized. Foam on the glass level also supports segregation of fine silica particles (silica scum). Temperature decreases foam stability as well as reducing components in atmosphere. The oxy-fuel combustion increases the water partial pressure in the atmosphere and enhances foaming [4]. The model predicting the foam layer thickness and its structure in laboratory conditions has been formed by Laimböck and Beerkens [5]. The foam models under real conditions face the problem of unknown foam properties such as density, viscosity and effective heat conductivity.

When the bubble release rate from the melt is higher than the collapse rate at the surface of the melt, or if the melt reacts with atmosphere forming bubbles (see next paragraph), foam rises on the glass level. According to Kappel, Conradt and Scholze [6], the ratio between surface tension and viscosity of glass plays a role in evaluating the foam stability. The glass foam behaves mostly as unstable, however, there are also properties characterizing metastable foam (foam with film elasticity supported by the adsorption of surface active component on the foam lamellae). The rate determining the process of foam decay is probably a tear process (succeeding foam drainage). No unified theory of foaming was developed, however, the most effective parameters are defined in this work [6]:

- increasing temperature destabilizes the foam
- increased pressure enhances foam decay
- enhanced evaporation from the glass destabilizes the foam
- foams containing SO_2 have short life times.

Interaction of gases on the glass level

The gas transport by diffusion in the liquid phase and surface reaction can control the specific mass flow of the *i*-th gas component on the glass level:

$$\frac{dm_i}{d\tau} = - \frac{k_i D_i}{k_i \delta_i + D_i} \Delta c_i, \qquad (1)$$

where k_i, D_i and δ_i are the reaction constants, diffusion coefficient and diffusion layer thickness of the i-th gas component, respectively, and Δc_i is its concentration difference between interfacial boundary and bulk of glass.

The transport of physically and chemically dissolved gases on the level is mostly controlled by diffusion ($k_i \delta_i >> D_i$),

$$\frac{dm_i}{d\tau} = - D_i \left(\frac{\partial c_i}{\partial z} \right)_{z=0} = - \frac{D_i}{\delta_i} \Delta c_i . \qquad (2)$$

The concentration gradient of the i-th gas component on the level is obtainable from the dissolved gas transport in the liquid phase [7 - 9]:

$$\frac{\partial c_i}{\partial \tau} = D_i \nabla^2 c_i - v \nabla c_i + \omega_i , \qquad (3)$$

where $\partial c_i / \partial \tau = 0$ under stationary conditions, the first term on the right side of equation (3) represents the mass transport by diffusion, the second one expresses the convection transport and the last one the contribution by the shifting of chemical equilibrium of a gas in the melt. If a gas is only physically soluble, only the first term on the right side of equation (3) should be considered otherwise the convection and shifting of appropriate chemical equilibria should be taken into account, too. The evaporation of SO_2 and O_2 from sulphates containing glass and the subsequent formation of Na_2SO_4 in the furnace atmosphere can be of technological importance here.

Two phenomena on the glass level can be controlled by a chemical reaction. At high partial pressures of water vapour in the atmosphere (oxy-fuel melting), the sulphate ion reaction with water vapour probably controls at least the first stage of rapid foam formation on the level of a glass melt containing sulphate ions [10]:

$$H_2O\ (g) + SO_4^{2-}\ (l) \rightleftharpoons \rightleftharpoons SO_2\ (g, l) + 1/2\ O_2\ (g, l) + 2\ OH^-\ (l) . \qquad (4)$$

The initial mass transport is proportional to $k\Delta c$, where Δc is the concentration difference of water or sulphate ions on the level. In the later stages of foaming, the mass transport of sodium sulphate ions or hydroxyl groups in the glass can also play a role and equation (1) is valid. At sufficiently high partial pressures of SO_2 and O_2 in the atmosphere, or when the glass melt is supersaturated by sulphates, the sulphate rich phase is precipitated on the glass level [11], this phenomenon being controlled by the diffusion of reaction components from the glass side and by the formation of sulphate ions from the gas side [12]. The following expression can be proposed for the thickness of the sulphate rich layer $\delta_{SO_4^{2-}}$:

$$\frac{d\delta_{SO_4^{2-}}}{d\tau} = \frac{1}{\rho_{Na_2SO_4}} \left[k_{SO_4^{2-}} (p_{SO_2} p_{O_2}^{1/2} - p_{SO_2 s} p_{O_2 s}^{1/2}) - \frac{M_{Na_2SO_4}}{M_{SO_2}} D_{SO_2} \left(\frac{\partial c_{SO_2}}{\partial z} \right)_{z=\delta} \right] , \qquad (5)$$

where $\rho_{Na_2SO_4}$ is the density of the sulphate rich layer, $k_{SO_4^{2-}}$ is the rate constant of the reaction of sulphate ion formation, and $M_{Na_2SO_4}$ as well as M_{SO_2} are the appropriate molecular weights. While the first term on the right side of equation (5) expresses the control by the chemical reaction - where p_i are the actual partial pressures of SO_2 and O_2 in the atmosphere and p_{is} are their partial

pressures in equilibrium with the sulphate layer - the second term assumes the sulphate layer growth or dissolution controlled by the diffusion transport of SO_2 in the melt. The SO_2 concentration distribution in the melt (see equation (3)) is needed to calculate the value of

$$\left(\frac{\partial c_{SO_2}}{\partial z}\right)_{z=\delta}.$$

If the layer is formed or present, the absorption or desorption rates of SO_2 and O_2 are by about three to four orders of magnitude greater compared with transport by diffusion in the glass. This is obvious from figure 2 where the rate of gas absorption by the liquid glass is represented by the rate of glass level increase in the small one side closed vessel containing the absorbed gas (O_2) or gas mixture of SO_2 and O_2 [12].

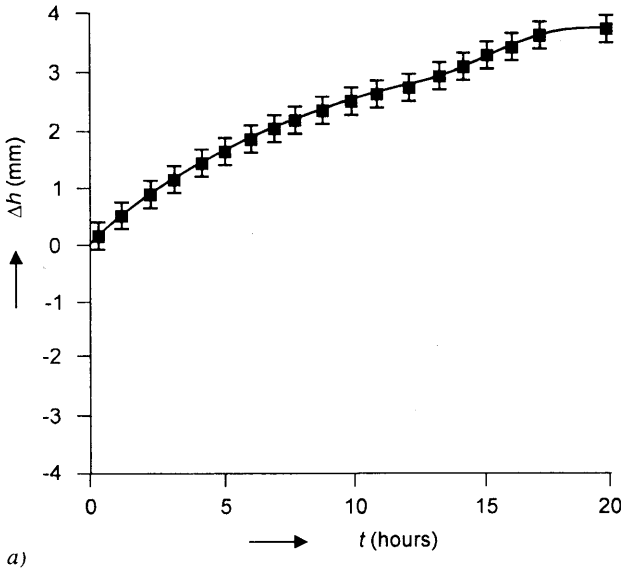

Figure 2. The shifting of the glass level in the vessel caused by absorption of gases in the glass melt at 1200 °C (increasing h indicates gas absorption).
a) oxygen; *b*) mixtures of SO_2 and O_2; ■ - 25 SO_2 + 75 O_2, ◊ - 50 SO_2 + 50 O_2, ▲ - 75 SO_2 + 25 O_2 (vol.%)

Interactions of bubbles with glass

The bubble removal from a glass melt is a significant technological problem. Therefore extensive attention has been paid to its solution [8-9, 13-24]. The bubble under real conditions of glass melting is mostly multicomponent, exhibiting intensive mass transfer with the melt, the diffusion transport of gases through the bubble boundary being usually the rate controlling phenomenon. The problem of multicomponent bubble removing from glass involves the following theoretical aspects:

- the angular convection around a bubble as a consequence of bubble rising
- the radial convection around the bubble as a consequence of moving bubble boundary (dissolution or growth of a bubble)
- the participation of a chemical reaction on the mass transfer between the bubble and glass melt.

The first studies ignored the angular convection dealing with a stationary bubble. The quasi-stationary approximations (13-15) neglected the motion of the bubble boundary (the radial convection) when solving the convective diffusion equation and a simplified differential equation has been used to determine the boundary motion. The time dependent concentration field of dissolved gas around a bubble was obtained. The quasi-steady solutions neglected both the radial motion of the bubble boundary and the time development of the concentration field around the bubble [16], providing thus a less realistic picture of bubble behaviour when compared with the quasi-stationary solutions.

The problem of rising bubbles was examined especially by using the Levich's steady state solution [17] for the mass transfer from a rising bubble [18 - 20]. Itoh, Yoshikawa, and Kawase [21] presented the model of a rising bubble using the quasi-stationary approximation. The model seems to be more realistic during the very early stages of bubble rising but gives very similar results with the quasi-steady solutions [20] in the later stages.

The problem of an oxidation-reduction reaction on the bubble boundary has been discussed and solved in [16, 18, and 22]. Beerkens and de Waal [23] obtained the concentration profile of oxygen in a glassmelt with the oxide refining agents indicating steeper course than that without refining agents and later Beerkens examined release and/or input of gases out or in rising bubbles under isothermal as well as non-isothermal conditions [24]. The steady state approximation was used [18 and 22] and the quasi-stationary approximation is probably found in [24]. The quasi-stationary solution of a stationary bubble with the oxidation-reduction reaction on its surface was also used by Simonis, [7] and solved by Yoshikawa and Kawase [8].

Holmquist has shown [11] that the sulphate rich phase can be precipitated on glass surfaces if a glass is supersaturated by sulphates or the melt containing alkali oxides is in contact with atmosphere containing high concentrations of SO_2 and O_2. The problem was treated for the sulphate layer on the bubble surfaces [12, 25].

In the following analysis, the equations will be presented applying the steady-state approximation for the gas concentration distribution around a rising bubble [17], taking into account the redox reactions in the glass [9] and if need be the sulphate layer precipitation on the bubble surface [11, 12, 25].

Both gravitational and centrifugal forces can play a role in the removal of bubbles, but the natural way is their rise in the gravitational field. As the present surface active components of glass immobilize, in most cases, the bubble boundary [26], the Stokes' equation for the bubble rising velocity is usually applied. The change of bubble size significantly influences this removal process. The bubble growth or dissolution can be evaluated by the help of the relationship between partial pressures of present gases in the bubble, p_i, and their equilibrium partial pressures in the melt, $p_{i\,Glass}$:

$$\sum_{i=1}^{n} p_i \gtrless \sum_{i=1}^{n} p_{i\,Glass} \quad . \tag{6}$$

Thus the upper inequality designates the bubble dissolution and the lower one its growth. As the values of p_i decrease with increasing number of present gases, it is difficult to dissolve multicomponent bubbles. If non-diffusing gases are present, the partial pressures of dissolving gases in the bubble decrease with time and dissolution stops in later stages.

The bubble growth or dissolution is controlled by the similar phenomena as in the case of mass transport through the glass level.

For the single multicomponent bubble rising through the non-isothermal melt, the derivative of Gay Lussac's equation gives:

$$\left[\rho g \frac{dZ}{d\tau} - \frac{2\sigma}{a^2} \frac{da}{d\tau} \right] 4/3\pi a^3 + $$
$$+ 4\pi a^2 \frac{da}{d\tau} (p_{ex} + \rho g Z + 2\sigma/a) =$$
$$= \sum_{i=1}^{n} \frac{dm_i}{d\tau} \frac{RT}{m_i} + \sum_{i=1}^{n} \frac{m_i R}{M_i} \frac{dT}{d\tau} \quad , \tag{7}$$

where Z is the bubble depth under glass level, a is the bubble radius, p_{ex} is the external pressure, m_i is mass of the i-th gas in the bubble, and ρ and σ are glass density and surface tension, respectively.

The corresponding equations can be written for each single gas present in the bubble or in the glass. The diffusion mass flow through the bubble surface in the steady state [17] is given by:

$$\frac{dm_i}{d\tau} = 4\pi a^2 \frac{0.381\,(m_{ib}-m_{ia}) D_i^{2/3} g^{1/3} \rho^{1/3}}{\eta^{1/3}} \quad , \tag{8}$$

where m_{ib} and m_{ia} are mass concentrations of the i-th gas in the bulk glass and on the bubble surface, respectively. The bulk concentration of chemically dissolved gases can be obtained from consideration of its chemical equilibrium with the appropriate complex ion in the melt and from its simultaneous transfer by diffusion and glass convection in the steady state:

$$K_{Me} = \frac{[Me^{a+}]^{4/b}\,[O_2]}{[Me^{(a+b)+}]^{4/b}} \quad , \tag{9}$$

$$D_i \nabla^2 c_i - v \nabla c_i + \omega_i = 0 \tag{10}$$

where K_{Me} is the equilibrium constant, and the quantities in brackets are the activities or concentrations of appropriate components of the oxidation-reduction reaction. Equation (10) expresses the simultaneous component transfer by diffusion (1st term), convection (2nd term) and the corresponding shifting of the chemical reaction (3rd term) into a steady state.

If the sulphate layer is precipitated on the bubble surface, the mass flow of SO_2 and O_2 through the bubble surface is given by [25]:

$$\frac{dm_i}{d\tau} = -4\pi a^2 A k_{SO_4^{2-}} [p_{SO_2} p_{O_2}^{1/2} - p_{SO_2 s} p_{O_2 s}^{1/2}] \quad , \tag{11}$$

where $k_{SO_4^{2-}}$ is the rate constant of the reaction of sulphate ion formation and p_i and p_{is} are the actual partial pressures of both gases in the bubble and their partial pressures in equilibrium with the sulphate layer, respectively.

The resulting set of differential equations includes the time derivative of bubble radius, partial pressures of single gases in the bubble and the change of the thickness of sulphate layer if present:

$$\frac{da}{d\tau}, \frac{dp_i}{d\tau}, \frac{d\delta_{SO_4^{2-}}}{d\tau} =$$
$$= F[(m_{ib} - m_{ia}) ; (p_{SO_2} p_{O_2}^{1/2} - p_{SO_2 s} p_{O_2 s}^{1/2})] \quad . \tag{12}$$

The values of m_{ib} for chemically dissolved gases are obtained by solving equations (9 - 10).

The transport of SO_2 and O_2 is controlled by diffusion if the sulphate layer is absent or if the partial

pressures of SO_2 and O_2 in the bubble are low. The set of equations is completed by the Stokes's equation for the bubble rising velocity and by the definition of the total pressure inside the bubble:

$$p_{ex} + \rho g Z + 2\sigma/a = \sum_{i=1}^{n} p_i \quad , \tag{13}$$

where p_{ex} is the external pressure and σ is the surface tension of glass. The difference between bubble radius development calculated according to equation (7) for the case when the formation of sulphate layer is or not considered can be seen in figure 3. The abrupt contraction of the bubble is obvious after layer formation. This fact predestines bubble different time-space history in a furnace. The calculations of bubble history in the melting space are needed to find out the actual technological significance of this phenomenon.

The experimental examinations of bubble radius development at constant temperatures show the almost linear growth in the later stages of refining which fact corresponds to the lower inequality sign in relation (6) (see figure 4, [27]) and to constant bubble composition. If temperature is sufficiently high, only diffusion of the refining gas is important and the influence of the main refining factors - as temperature, pressure, and composition - can be easily derived [28].

The simplified theoretical temperature dependence of the refining time of the bubble in a static isothermal glass layer exhibits a steep exponential decrease with increasing temperature which fact is in agreement with results of experiments [28]. The comparison between the mentioned theoretical dependence and the dependence based on the experimental values of bubble growth rates

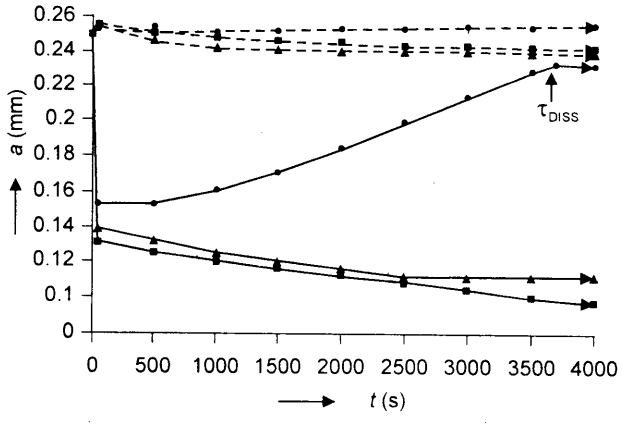

Figure 3. Bubble radius as a function of time in soda-lime-silica glass melt: 74 SiO_2, 16 Na_2O, 10 CaO (wt.%). The initial composition of the bubble: 60 SO_2 , 30 O_2 , 10 CO_2 (vol.%). τ_{Diss} - the dissolution time of the sulphate layer, —— including sulphate layer, — — — gas diffusion controlled only, ■ - 1100 °C, ▲ - 1200 °C, ● - 1300 °C

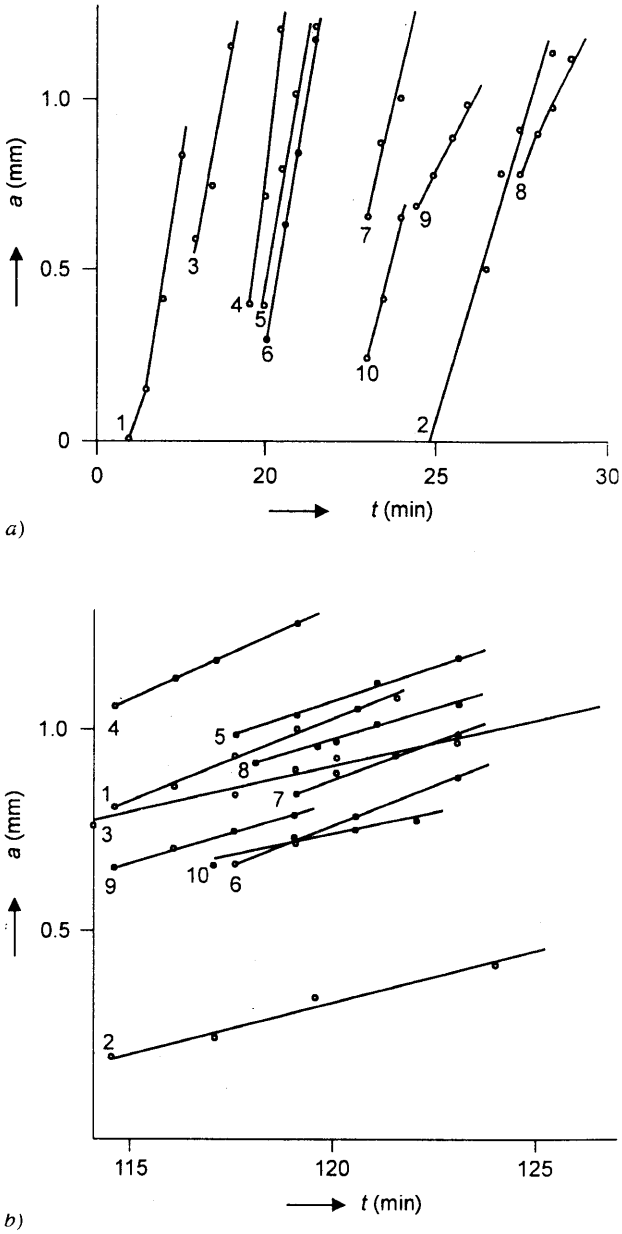

Figure 4. The linear bubble growth at refining temperatures. *a*) soda-lime-silica glass with 0.5 wt.% Na_2O as Na_2SO_4 at 1450°C, *b*) borosilicate glass with 1 wt.% Na_2O as NaCl at 1560 °C

is in figure 5. The simplified theoretical dependence of the refining time on pressure shows a hyperbolical decrease of the refining time with decreasing external pressure. This fact is presented in figure 6 [28]. Among the impact of glass basicity, refining agent concentration, and the redox state of glass on the refining behaviour, the redox influence is of the greatest interest. The simplified dependence between the refining time of a bubble in the isothermal static glass and the redox state of glass in oxidized and slightly reduced glasses is given by [28]:

$$\tau_R = \frac{1}{(K_1 / [O_2]^{1/2} + K_2 [O_2] - K_3)^{2/3}} \qquad (14)$$

where K_1 - K_3 are constants and $[O_2]$ is the concentration of physically dissolved oxygen in a glass melt.

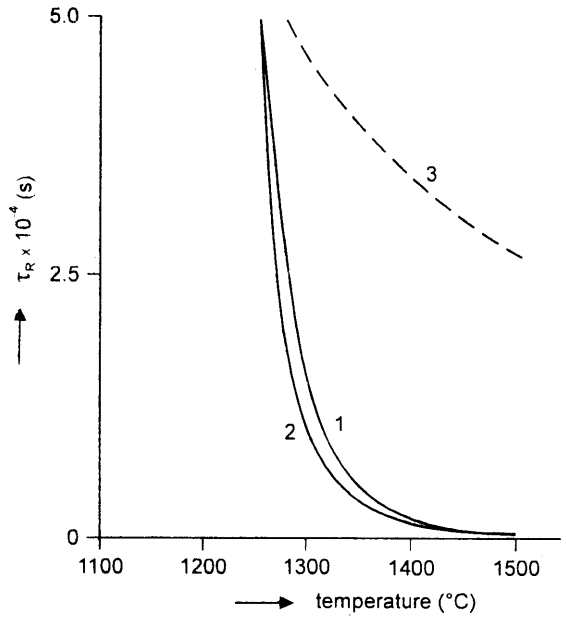

Figure 5. The temperature dependence of the refining time, τ_R, soda-lime-silica glass with sulphate refining agent, the initial bubble depth under glass level 1m, $a_0 = 5 \times 10^{-4}$ m.
1 - the theoretical equation, 2 - the $\tau_{R(T)}$ course using the experimental values of bubble growth rates; — — — no refining agents

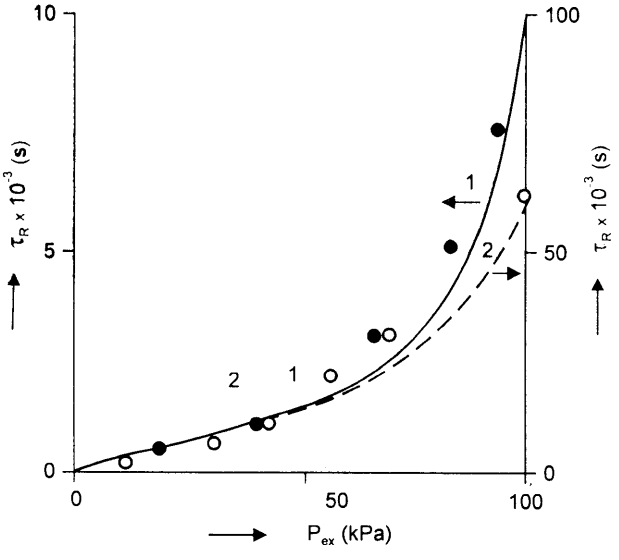

Figure 6. The dependence between the refining time of a bubble, τ_R, and external pressure, p_{ex}, for TV glass, temperature 1400 °C, $h_0 = 1$ m, $a_0 = 1 \times 10^{-4}$ m.
1 - with antimony as a refining agent, 2 without any refining agents; ——— theoretical equation, O ● the course using experimental values of bubble growth rate

For the oxide refining agents (As_2O_3 and Sb_2O_3), the term with $[O_2]^{1/2}$ is absent and the value of τ_R decreases with increasing redox state of glass [9]. For the sulphate refining agent, however, τ_R decreases as well at low values of the redox state of glass as the term $K_1/[O_2]^{1/2}$ increases. The main refining gas in this redox state region is SO_2 (flint glasses, amber glasses). The calculated dependence between the bubble refining time in the soda-lime-silica glass refined by sodium sulphate and the initial redox state of glass brings figure 7 [9].

The modelling of bubble behaviour under non-isothermal conditions according to equations (12 - 13) requires a lot of data, especially the temperature dependences of diffusion coefficients of gases, gas solubilities and equilibrium constants of reactions by which the appropriate gases are bound in the glass. The bubble growth rates may be, on the other hand, relatively simply experimentally measured and their values are almost independent from time and bubble size in the later stages of experiments [29]. The temperature dependence of the average value of bubble growth rate and the Stokes' equation can be therefore used to model the bubble behaviour under non-isothermal conditions of flowing glass. The contribution to the bubble growth or dissolution brought about by the variations in the amount of refining gas in the bubble under non-isothermal conditions, is approximately given by [29]:

$$\left(\frac{da}{d\tau}\right)_C = \frac{a\, dC}{300 - C\, d\tau} \,, \qquad (15)$$

where C is the percentual volume concentration of the refining gas in the bubble. The rate of change of bubble composition can be obtained from laboratory observations of bubble shrinkage when abruptly decreasing temperature and from the modelling of bubble history in a melting space.

In spite of the considerable complexity of bubble problem in glass melts, some phenomena as is evaporation of volatile components (PbO, B_2O_3, As_2O_3 etc.) into bubbles and the mass transport of reducing gases (CO and H_2) present in some bubbles are not involved, yet. The contribution of volatile components to the bubble growth rates in lead and borate glasses can be, however, non-negligible; the knowledge of chemisms and mechanisms of CO_2 and H_2 behaviour in bubbles and in the melt can help with identification of bubble sources in glass melting furnaces.

To describe completely the impact of bubble behaviour on the glass quality, the concentration fields of bubbles inside of a melting space are very useful. Balkanli and Ungan [30] predicted the density and size distribution of CO_2 bubbles in the melting space by solution of the appropriate continuity and conservation

equations. It seems, however, that the numerical solution of the real multicomponent bubble using this procedure will be too complicated and time consuming. In addition, very little is known about number and size distribution of bubbles entering the glassmelting space and coming from different bubble sources. The further work in this area is needed [31].

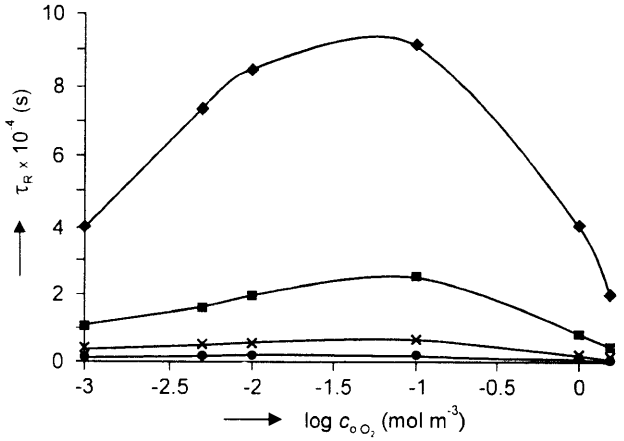

Figure 7. The dependence between the refining time of a bubble and the value of the initial redox state of the soda-lime-silica glasses containing sodium sulphate, h_0 = 0.1 m, a_0 = 1 × 10^{-4} m.

Bubble nucleation in glass

The appropriate relations giving the rate of bubble nucleation and growth of bubble nuclei were given by Izumitani and Terai [32]. According to authors, the decrease of thermodynamic barrier of the heterogeneous bubble nucleation is given by:

$$A_k^* = \frac{16\pi\sigma^3}{3\eta}\left[\frac{1-\ln c/c_0}{p_{ex}-\ln c/c_0}\right]^2 \frac{1}{4}(2-\cos\Theta)\,(1+\cos\Theta)^2 \,, \quad (16)$$

where c_0 and c are the concentrations of gas in the saturated and supersaturated solution, respectively, and Θ is the contact angle between the liquid and solid phase. Thus, if heterogeneity is not wetted ($\Theta = \pi$) by the melt, the energetic barrier has maximum value corresponding to the homogeneous nucleation. The experimental observations have shown [26] that bubble nucleation in glasses has heterogeneous nature and the thermodynamic and kinetic barriers of bubble nucleation should be probably low. The knowledge of the internal partial pressure of gases in the glass melt under the given conditions is therefore useful to find potential conditions of bubble nucleation, i.e.:

$$p_{i\,melt} \rangle p_{ex} + \rho g Z \,. \quad (17)$$

If the condition (17) is fulfilled, i.e. glass is supersaturated, the bubble nucleation can be expected. The values of $p_{i\,melt}$ can be generally obtained by the solution of equation (3) and by applying Henry's law. As may be expected, especially refining gases cause bubble nucleation in glass melts. Figure 8 presents the calculated values of $p_{O_2 melt}$ as the function of the initial redox state of glass at two temperatures. The regions of redox values can be defined at both temperatures according to inequality (15) where the bubble nucleation can occur. However, to describe the actual intensity of the bubble nucleation process, the more detailed experimental and theoretical work is needed.

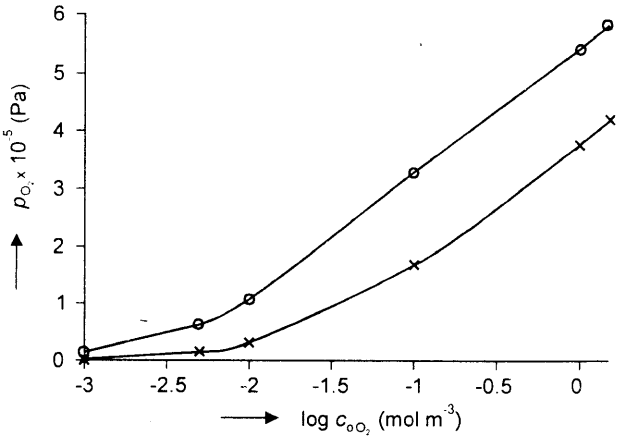

Figure 8. The dependence of the internal partial pressure of O_2 in the TV glass, p_{O_2}, on the value of the initial redox state of glass.
× - 1400 °C, O - 1500 °C

Bubble evolution from solid materials

The most frequent sources of bubbles are heating electrodes and refractory materials. The origin of bubbles on the electrodes is electrolytic or bubbles are the consequence of glass superheating and supersaturation by the refining gas close to the electrode. Only qualitative observations of bubble formation and growth on the electrodes have been performed [33].

The main mechanisms of bubble generation were summarized by Swarts [34]:

1. Mechanisms evoked by the refractory material porosity.

The evident mechanism is opening of closed pores by the material corrosion. The volatile components of glass evaporate into a opened pore, form a viscous melt, facilitate the wetting of inner pore surface and consequently, glass easily fills the pores. The gases in the pores could be sometimes under pressure and bubbles are expulsed from the material. The main gases are CO_2 and

N_2, however, the bubbles quickly react with the melt and the original bubble composition is changed.

The thermal transpiration is a mechanism exhibited by materials with opened porosity [35]. The existence of thermal gradients across the material (across the length of pores) leads to a pressure gradient in the pores. The gas flow from the colder part of the pore to the hotter one (glass-material contact) is a consequence of this temperature distribution. The hydrostatic pressure at the pore-glass contact location can balance the gas expulsion and bubble formation. The capillary force can as well push the gas into a melt if an opened pore contacts the glass melts by both its ends and the pore orifices have different diameters.

2. Mechanism evoked by the exudation of refractory materials glassy phase.

The vitreous phase originated during refractory block fabrication becomes mobil at glass melting temperatures, its fluidity increases by the reaction with alkali from the glass and the exuded glassy material then mixes with the glass melt [36]. The bubbles can be generated by the change of glass redox state, glass basicity or by reaction with impurities.

3. Reactions with impurities.

- reaction with nitrides which produces bubbles with high content of nitrogen. The oxidation reaction can use both oxidation species of a glass melt and oxygen diffusing through the material from atmosphere. Mathematical modelling could help in identification of the source as the bubble composition only slowly changes with time.
- reaction with iron; In the elemental or ferrous state, iron can reduce sulphates and provide bubbles with high content of SO_2. The s.c. "iron spots" containing Fe_2O_3 yield O_2 when reduced [37]. The gas composition of oxygen bubbles quickly changes by oxygen dissolution in the glass and by diffusion of other gases into a bubble.
- reactions with subpaving.

Tanks having long service can suffer from penetration of glass melt between pavers and from the subsequent reaction with the clay subpaving. The rapid clay dissolution and the following decrease of glass basicity leads to the decomposition of sulphates, if present [38].

4. Electrolytic reactions.

The oxygen bubbles produced on zircon refractory-glass interface are consequence of the $O^{2-} \rightarrow O_2$ conversion [39 - 41]. The electromotive force on the surface of the material is evoked by the difference of alkali content in the glass and refractory material. The mentioned conversion is accompanied by reduction of impurity cations (Fe^{3+}, Ti^{4+}) within the refractory. Electric charge is transferred both by electrons and alkali species. With decreasing the interface alkali difference (time, pretreating the refractory surface with alkali) or with stopping electron migration by application of a bulking potential, the O_2 generation slows down.

No mathematical models describing the bubble formation by the mentioned interactions were proposed up to now. Their creation, however, is needed to findout the relation between glass quality and melting process conditions.

Interaction of bubbles with highly viscous and solid glass

The works of Golob and Swarts [42] and others [43 - 46] dealt with the nature and origin of condensates inside of bubbles in cooled glass, especially with those arising in the bubbles containing SO_2 and coming from the sulphate containing glasses. The experiments of Golob and Swarts proved the disproportionation reaction of SO_2 accompanied by the alkali transport from the glass was responsible for the sulphate and sulphur condensates inside of bubbles:

$$3\ SO_2\ (g) + 2\ Na_2O\ (l, s) \rightleftharpoons 2\ Na_2SO_4\ (l, s) + 1/2\ S_2\ (g, l)\ . \qquad (18)$$

This reaction did not work at 1300 °C according to [12] but occurred already at 1100 and 1200 °C as demonstrated Golob and Swats [42]. It was reported in [46] that the reaction between SO_2 and interior of the soda-lime-silica capillars took place as well at temperatures bellow T_g (300 - 500 °C). Thus, not only gas shrinking but also condensation reaction (16) influences the total pressure inside bubbles, which is an important bubble property when searching for the bubble sources in glass furnaces.

The behaviour of a bubble in the temperature interval where the bubble is "frozen" in glass can be described in a simplified way by the time-pressure dependence:

$$\frac{dp}{d\tau} = R\ \frac{dT}{d\tau}\left(\sum_{i=1}^{n-1}\frac{c_{if}}{100V_{mf}} + \frac{c_{SO_2 f}}{100V_{mf}}\right) + \frac{1}{4/3\pi a_f^3}\ \frac{dn_{SO_2}}{d\tau}\ RT\ , \qquad (19)$$

where p is total pressure, $dT/d\tau$ is the rate of glass cooling, c_{if} is the volume percentage of the i-th gas in the bubble at temperature of bubble "freezing" in the glass, V_{mf} is the molar volume of gas at this temperature, a_f the final bubble radius and n_{SO_2} is the number of moles of SO_2 in the bubble in given time.

The rate of SO_2 gas condensation may be controlled by the rate of reaction (18) or by the diffusion transport of Na_2O from glass to the bubble surface. The first case (assuming the first order chemical reaction) gives for n_{SO_2}:

$$n_{SO_2} = n_{SO_2,f} \exp(14\pi a_f^2 k_{SO_2} \tau) \quad , \tag{20}$$

where k_{SO_2} is the rate constant of the condensation reaction. If the condensation is controlled by the diffusion of Na_2O, the molar flow of SO_2 to the bubble surface is given by:

$$\frac{dn_{SO_2}}{d\tau} = \frac{6D_{Na_2O}\pi a_f^2}{M_{Na_2O}} \left(\frac{dc_{Na_2O}}{dr}\right)_{r=a_f} . \tag{21}$$

The value of the concentration gradient on the bubble surface is obtainable from the solution of the second Fick's law.

According to [42], the diffusion transport of Na_2O is most probably the controlling mechanism, however, chemical reaction may be controlling too in the very early stages. Further experiments including reactions between SO_2 and alkali containing glasses are needed to establish the controlling mechanism and to form an adequate model of bubble behaviour at low temperatures.

VERIFICATION OF MODELS

The most significant model used to describe the interactions between gas phase and glass melt is the model of a multicomponent bubble in a glass melt. The reasonable theoretical predictions have practical consequence both for the refining process and for the identification of bubble sources in glass melting spaces. The comparative laboratory methods working with the artificial bubbles of defined initial properties (size and composition) make it possible to follow the bubble composition or the bubble size development under laboratory conditions. It is supposed that the consent under simple laboratory conditions implies the identical behaviour also under real melting conditions. The methods of defined bubble production involve bubbling of the given gas or gas mixture into a melt, chemical preparation of CO_2 or SO_2 bubbles from tiny Na_2CO_3 or Na_2SO_3 crystals, melting of glass cullet in the defined atmosphere or exposure of the supposed bubble source (e.g. refractory materials) to the melt.

The mass spectrometric or gas chromatographic determination of gas content of a bubble and the microscopic or X-ray diffraction examinations of condensates are used most frequently to compare the experimental bubble composition changes with the models [42]. The visual high temperature methods [47] are applied to examine experimentally the bubble growth or dissolution in the glass melt. The discrepancy between experiments and theoretical description can be caused either by simplifications of applied theoretical description or by the accuracy of the experimental gas data entering the model (gas concentrations, solubilities, diffusion coefficients and equilibrium constants of the appropriate chemical reactions). The accuracy of the mentioned data seems to be the crucial problem of the satisfactory bubble model application. Figure 9 brings the comparison between the theoretical and experimental bubble composition developments in soda-lime-silica glass melt.

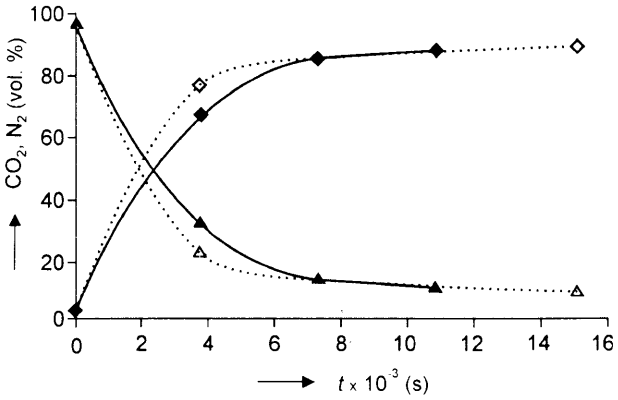

Figure 9. Bubble composition developments (CO_2, N_2) in the soda-lime-silica glass (74 SiO_2, 16 Na_2O, 10 CaO (wt.%)) at 1300 °C. Comparison between the mathematical model and results of bubble analyses.
· · · · mathematical model, ——— results of bubble analyses, ♦ - CO_2, ▲ - N_2

APPLICATIONS

Intensification of the refining process

The single bubble tracing through the examined glass melting space helps to evaluate the influence of condition variation on the course of the refining process. The following figure 10 shows the impact of the initial redox state of glass (given by the concentration of physically dissolved oxygen) on the maximum X-coordinate where the bubble coming from the batch layer in a horizontal melting tank reaches the glass level. Curve 1 shows the bubble behaviour in the soda-lime-silica glass refined by the sodium sulphate, curve 2 the behaviour of the same starting bubble in the TV glass refined by antimony. The courses of both curves are in a qualitative consent with the simplified dependence between the refining time and redox state of glass under isothermal conditions, given by equation (14) and figure 7.

The development of a sulphate layer on the bubble surface can also alter the bubble history in a melting furnace. This is obvious from figure 11.

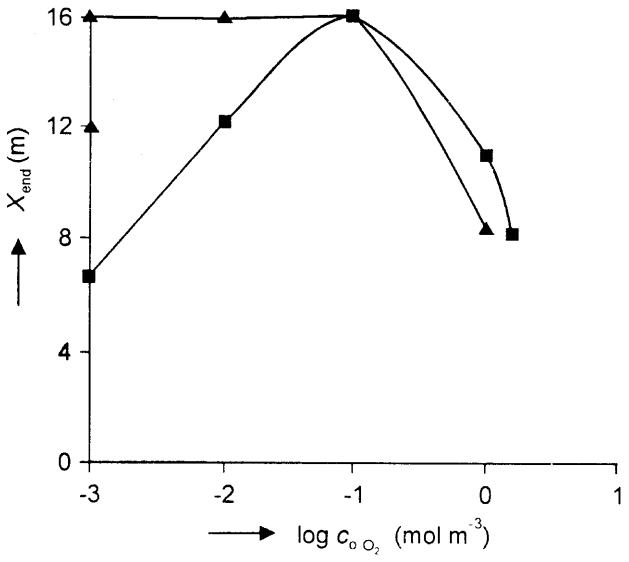

Figure 10. The X-coordinate of a bubble when reaching the glass level, X_{end}, as a function of the initial redox state of glass, a_0 = 0.1mm, c_{0CO_2} = 95 vol.%, c_{0N_2} = 5 vol.%, starting point 0.6, 2.2, 0.2 (m).
■ - soda-lime-silica glass refined by sodium sulphate, ▲ - TV glass refined by antimony

Prediction of furnace design using modelling

Not only melting conditions but also the size and shape of a melting space can be properly designed by using the modelling procedure. In an experimental and theoretical study of refining under reduced pressure, the proper temperature and pressure of refining were found by laboratory experiments and the simplified model of bubble behaviour (see equation (15)) was applied to trace bubbles in the refining channel. In figure 12, the curve 1 defines temperatures and pressures for the bubble growth rate 10^{-6} m s^{-1} (a value sufficient for the effective refining), the curve 2 defines the bubble nucleation on the Pt walls of the channel and temperature 1200 °C indicates the stable foam at lower temperatures. These mentioned lines characterize the area IV as the most convenient for the effective refining without bubble nucleation and foaming. The following figure 13 provides the results of bubble tracing of the modelled refining channel, being 2 m long, 0.4 m wide and having 0.15 m thick layer of flowing glass, by bubbles starting in the central longitudinal section of the channel. The value of X_{final} designates the X-coordinate of a critical bubble when reaching the glass level. If X_{final} < 2 m, the bubble is removed from the channel. As is obvious from this figure, much lower temperatures are needed in the case of presence of refining agent to ensure glass refining than is declared by figure 12. The same is valid for the glass without any refining agent. As temperatures should be greater than about 1200 °C (see figure 12, the temperature of stable foam), a considerable refining reserve exists in the channel. The decrease in length of the chanel can be a construction change utilizing this reserve.

The regions of potential bubble nucleation in a glass melting space

Using the calculation of redox distribution inside of a glass melting space (equations 9 and 10), the regions of gas supersaturation in the melting space can be defined. The example presented in figure 14 brings the isobars representing the sum of internal partial pressures of SO_2 and O_2, $p_{SO_2melt} + p_{O_2melt}$, valid for the soda-lime-silica glass with 0.50 wt.% Na_2O as Na_2SO_4. As SO_3 is the primary decomposition product of sulphates which almost completely dissociates to SO_2 and O_2, the bubble nucleation can be expected when $p_{SO_2melt} + p_{O_2melt} >$ > 150 kPa + ρgZ. As is obvious from figure 14, this condition is fulfilled in the level region of maximum temperatures. The unknown thermodynamic data hinder the calculation of glass supersaturation in the regions of decreasing glass basicity, resulting from the refractory material dissolution in the melt.

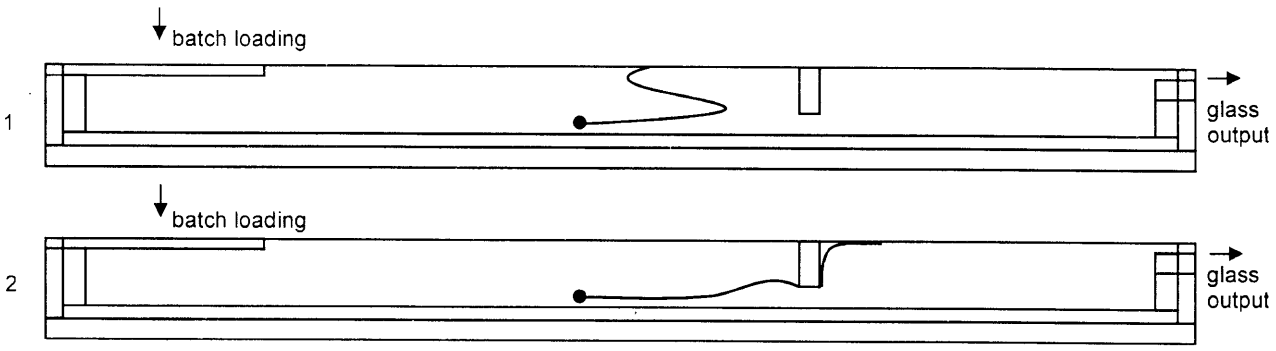

Figure 11. The projections of bubble trajectories in the vertical longitudinal section through the model melting furnace, initial bubble radius 0.1 mm, c_{0CO_2} = 10 vol.%, c_{0SO_3} = 60 vol.%, c_{0O_2} = 30 vol.%, ● - initial bubble position: X_0 = 7.5 m, Y_0 = 4.0 m, Z_0 = 0.9 m. 1 - bubble behaviour controlled only by diffusion, 2 - including the influence of the sulphate layer

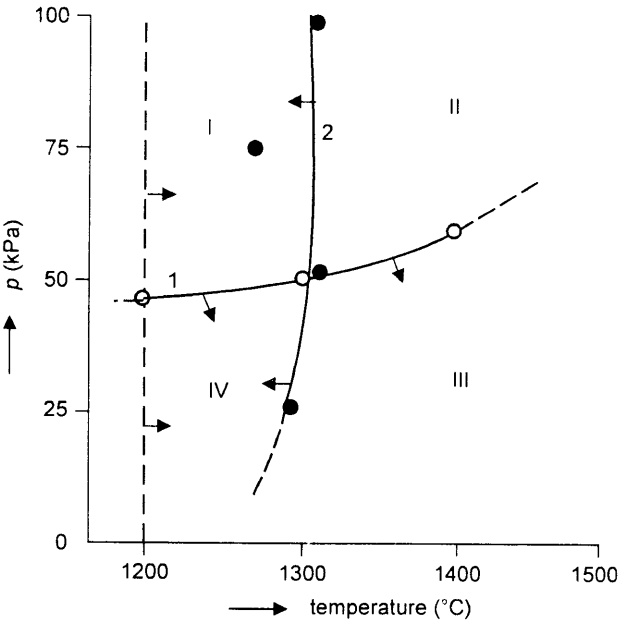

Figure 12. The definition of the temperature-pressure area, applicable for the refining in the refining space with lead-silica glass melt containing arsenic as the refining agent.
— — — the temperature of stable foam layer on the glass level; ○ - the curve defining the bubble growth rate 10^{-6} m s^{-1}, ● - the curve defining the bubble nucleation temperature

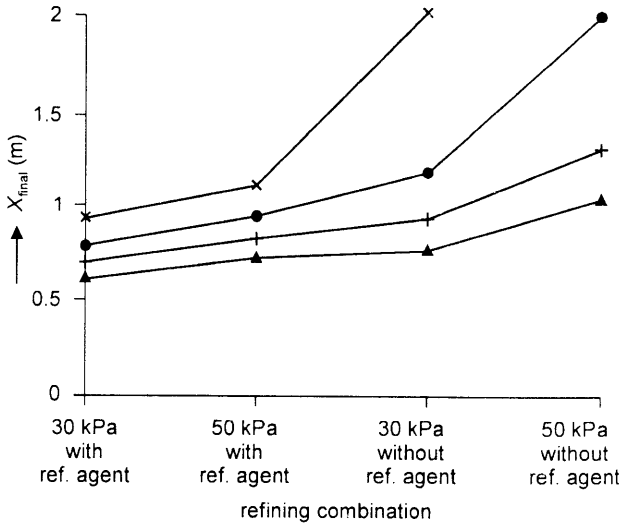

Figure 13. The maximum X_{final}-coordinate of critical bubble, when reaching the glass level (X_{final} = 2 m, bubble has not been refined). Refining under reduced pressure, output 3t per day.
× - 1150 °C, ● - 1200 °C, + - 1250 °C, ▲ - 1300°C

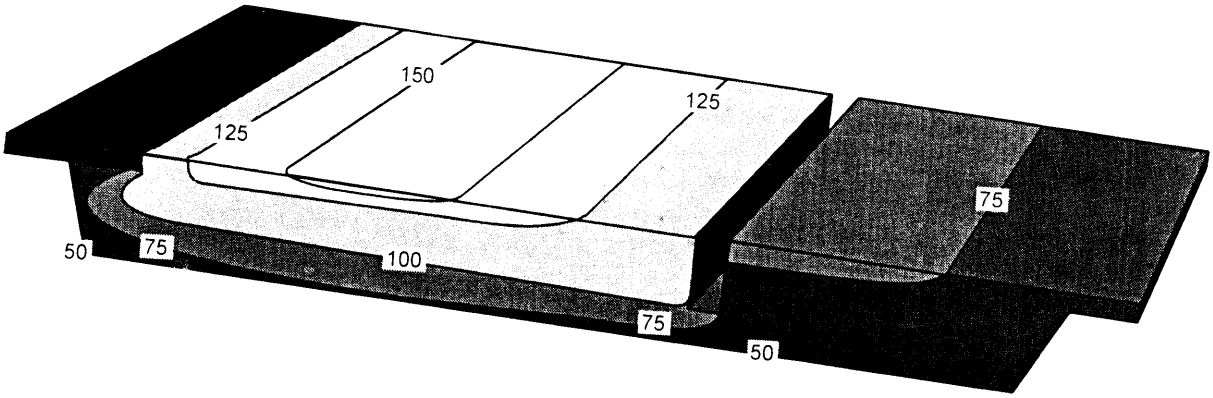

Figure 14. The isolines of $p_{SO_2melt} + p_{O_2melt}$ (kPa) in the model glassmelting space, NCS glass (0.5 wt.% Na_2O as Na_2SO_4).

Identification of bubble source location in a glass melting space using bubble tracing

The ability of a bubble source evaluation depends on the accuracy of bubble analysis and on the knowledge of bubble history. The preliminary modelling of bubble history gives a knowledge base of the most probable behaviour of actual defect bubbles. The modeiling has been usually accomplished by the laboratory simulation of a bubble source and by observing the size and composition development of generated bubbles [48, 49]. The results of this laborious measurements are, however, dependent from the glass composition and the time-temperature history of a bubble as well as from the redox state of glass [9]. The mathematical modelling of bubbles released from their potential source seems to be the general identification tool if the model of bubble behaviour is complete (see equations (7), (12) and (13)), its reliability has been verified, and the fundamental information about the bubble source is known (location in the space and the most probable bubble initial composition). The consideration of the bubble history around transformation temperatures plays here a non-negligible role.

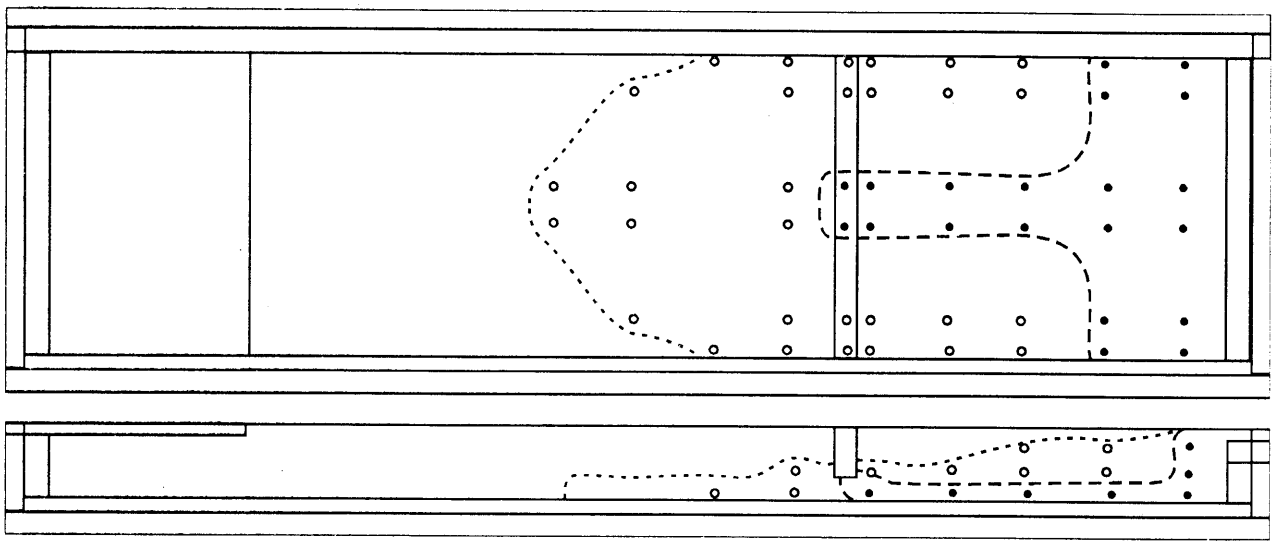

Figure 15. The probable region of an air bubble source in the model melting furnace.
$c_{CO_2} \in$ <60; 65>; $c_{N_2} \in$ <35; 40> (vol.%); $a^a \in$ <0.2; 0.6> (mm); $p^a \in$ <20; 22> (kPa)
— — — $c_{Ar} \in$ <0.2; 0.3>, · · · · · $c_{Ar} \in$ <0.01; 0.3> (vol.%)

In the modelling procedure, the assumed region of a bubble source in the melting space is mapped using the bubbles of given initial composition and different sizes. Only bubbles leaving the glass melting space with glass are considered. The bubble properties at the output (size, composition and pressure) are recalculated to the ambient temperature and form the comparative base for the actual defect bubbles. In figure 15, the probable region of the air source on the interface between refractory material and glass melt is indicated for the simulated bubble analysis: $c_{CO_2} \in$ <60; 65>, c_{N_2} <35; 40>, $c_{Ar} \in$ <0.2; 0.3> (vol.%), $a \in$ <0.2; 0.6> (mm), $p \in$ <20; 22> (kPa). The probable source region is in the working part of the model melting space.

The mostly insufficient accuracy of bubble modelling at melting temperatures, the scarce knowledge of condensation kinetics inside bubbles during cooling and the incomplete information about chemisms and mechanisms of bubble formation or releasing from the source prevent, however, from the wide contemporary applications of theoretical models in this technologically important area.

CONCLUSION

The verified and complete theoretical models of interactions between gases and glass melts (working under technological conditions) are a powerful tool when improving the melting process, increasing glass quality and palliating the undesirable effects of melting. The theoretical model of bubble behaviour at melting temperatures is almost complete, however, its verification is urgently needed. The remaining models are in the state of laboratory semiempirical descriptions (glass foaming, reactions on the glass level and bubble nucleation) or experimental examinations (bubble releasing from the refractory materials and electrodes) and their adjusting to real conditions is expected.

As the model verification is the final stage of any model application, the neccesary experimental methods should be developed or modified. These methods include especially measurements of gas properties in glasses, methods of bubble and foam production and treating in a laboratory scale and their evaluation as well as bubble and foam analyses.

Acknowledgement

This work was supported by the Ministry of Education, Youth and Sports of the Czech Republic, project No. VS 96 065.

References

1. Hrma P. in: *Chemistry of Glasses*, editor Paul A., p. 157-178, Chapman and Hall, London and New York 1988.
2. Kim D.S., Hrma P.: Ceram. Bull. *69*, 1039 (1990).
3. Hrma P., Kim D.S.: Glass Technol. *35* , 128 (1994).
4. Beerkens R.G.C.: Glastechn. Ber. - Glass Sci. Technol. *68*, 369 (1995).
5. Laimböck P., Beerkens R.: *Foaming of glass melts by decomposition sodium sulphate*. Presented at: The American Ceramics Society, Glass & Optical Materials Division, Fall Meeting 1994, Columbus, OH (USA).
6. Kappel J., Conradt R., Scholze H.: Glastechn. Ber. *60*, 189 (1987).
7. Simonis F.: Glastechn. Ber. *63K*, 29 (1990).
8. Yoshikawa H., Kawase Y.: Glastechn. Ber. - Glass Sci. Technol. *70*, 31 (1997).
9. Raková M., Němec L.: Ceramics – Silikáty *42*, 1 (1990).
10. Cable M., Rasul C.G.: J. Am. Ceram. Soc. *50*, 528 (1967).

11. Holmquist S.: J. Am. Ceram. Soc. *49*, 467 (1966).
12. Kloužek J., Němec L.: Glastechn. Ber. - Glass Sci. Technol. *68C*, 128 (1995).
13. Epstein P.S., Plesset M.S.: J. Chem. Phys. *18*, 1505 (1950).
14. Doremus R.H.: J. Am. Ceram. Soc. *43*, 655 (1960).
15. Krämer F.: Glastechn. Ber. *52*, 43 (1979).
16. Subramanian R.S., Chi B.: Chem.-Eng. Sci. *35*, 2185 (1980).
17. Levich V.G.: *Physicochemical hydrodynamics*, Englewood Chiffs, New York 1962.
18. Němec L.: Glass Technol. *21*, 134 (1980).
19. Onorato P.I.K., Weinberg M.C., Uhlmann D.R.: J. Am. Ceram. Soc. *64*, 676 (1981).
20. Ramos J.I.: J. Am. Ceram. Soc. *69*, 149 (1986).
21. Itoh E., Yoshikawa H., Kawase Y.: Glastechn. Ber. – Glass Sci. Technol. *70*, 8 (1997).
22. Němec L.: Glass Technol. *15*, 153 (1974).
23. Beerkens R.G.C., de Waal H.: J. Am. Ceram. Soc. *73*, 1857 (1990).
24. Beerkens R.C.G.: Glastechn. Ber. *63K*, 222 (1990).
25. Němec L., Kloužek J.: J. Non-Cryst. Solids *231*, 152 (1998).
26. Němec L.: J. Am. Ceram. Soc. *60*, 436 (1977).
27. Němec L.: Sklář a keramik *23*, 202 (1973). (in Czech)
28. Němec L.: Glastechn. Ber. - Glass Sci. Technol. *68*, 1, 39 (1995).
29. Kloužek J., Němec L. Ullrich J.: Proc. 4th International Seminar on Mathematical Simulation in Glass Melting, p.21, Horní Bečva June 16 – 17, 1997.
30. Balkanli B., Ungan A.: Glass Technol. *37*, 164 (1996).
31. Němec L.: Unpublished results.
32. Izumitani T., Terai R.: Advances in glass technol., Proc. 6th Internat. Congress on Glass, p. 205 (1962).
33. Matěj J.: Glastechn. Ber. *66*, 307 (1993).
34. Swarts E.L.: Glastechn. Ber. *65*, 87 (1992).
35. Edmonds T., Hobson J.P.: J. Vac. Sci. Technol. *2*, 182 (1965).
36. Mayer H., Pochnitzsch H.: Glastechn. Ber. *38*, 393 (1965).
37. Clark P.D., Ford W.F., Brett N.H.: Glass Technol. *15*, 39 (1974).
38. Chmielenski J.: Szklo Ceram. *14*, 322 (1963).
39. Bossard A.G.: USA pat. no. 2919209, Appl. Date Jan 4, 1955, publ. date Dec 29, (1959).
40. Bedroš P., Fojtková M.: Sklář a keramik *34*, 349 (1984). (in Czech)
41. Baucke F.G.K., Röth G.: Glastechn. Ber. *61*, 109 (1988).
42. Golob H.R., Swarts E.L.: J. Am. Ceram. Soc. *67*, 564 (1984).
43. Rosasco G.J.: Simmons J.H.: Am. Ceram. Soc. Bull. *54*, 590 (1975).
44. Minakov V.A., Min'ko N.I., Nesterenko G.T., Zhemela N.A., Vasyntin I.N., Kashirina E.F.: Glass Ceram. *33*, 482 (1976).
45. Minko N. I., Zhemela N.A., Nesterenko G.T.: Steklo No.1, 18 (1978). (in Russian)
46. Grim J., Knodler H., Schaefer M.A.: Verres Refract. *35*, 315 (1981).
47. Němec L., Kloužek J., Maryška M., Raková M., Šimůnková D.: Glastechn. Ber. - Glass Sci. Technol *68K*, 134 (1995).
48. Němec L., Ullrich J.: Glass *73*, 281 (1996).
49. Němec L., Ullrich J.: Internat. Glass Review No. 3-4, 60 (1996).

Submitted in English by the authors.